A three-dimensional monotonicity-preserving modified method of characteristics on unstructured tetrahedral meshes

Bassou Khouya[1,2,*] Mofdi El-Amrani[2,†] Mohammed Seaid[3,‡]

[1] *International Water Research Institute, University Mohammed VI Polytechnic, Benguerir, Morocco*
[2] *Laboratory of Mathematics and Applications, FSTT, Abdelmalek Essaadi University, Tangier, Morocco*
[3] *Department of Engineering, University of Durham, South Road, Durham DH1 3LE, UK*

Abstract

Slope limiters have been widely used to eliminate non-physical oscillations near discontinuities generated by finite volume methods for hyperbolic systems of conservation laws. In the current study, we investigate the performance of these limiters as applied to three-dimensional modified method of characteristics on unstructured tetrahedral meshes. The focus is on the construction of monotonicity-preserving modified method of characteristics for three-dimensional transport problems with discontinuities and steep gradients in their solutions. The proposed method is based on combining the modified method of characteristics with a finite element discretization of the convection equations using unstructured grids. Slope limiters are incorporated in the method to reconstruct a monotone and essentially non-oscillatory solver for three-dimensional problems at minor additional cost. The main idea consists in combining linear and quadratic interpolation procedures using nodes of the element where departure points are localized. We examine the performance of the proposed method for a class of three-dimensional transport equations with known analytical solutions. We also present numerical results for a transport problem in three-dimensional pipeline flows. In considered test problems, the proposed method demonstrates its ability to accurately capture the three-dimensional transport features without non-physical oscillations.

Keywords. Monotonicity-preserving schemes; Slope limiters; Finite element methods; Modified method of characteristics; Transport problems; Unstructured tetrahedral meshes

1 Introduction

Transport problems have been widely used in the literature to model many industrial, environmental and biomedical applications involving advection of scalar quantities such as density, temperature or concentration, among others. For example, transport problems have been used to describe water transfer in soils [22], heat transfer in a draining film [24, 39], and the transport of scalars in ferrofluids under rotating magnetic fields [5, 42]. On the other hand, several numerical schemes have been developed in the literature to solve the transport equations. Most of these techniques can be classified into three main categories (i) Eulerian methods, (ii) Lagrangian methods and (iii) semi-Lagrangian methods. In the finite element context, the most popular Eulerian methods include the streamline upwind Petrov-Galerkin

*khouya.bassou@um6p.ma
†mofdi.elamrani@urjc.es
‡m.seaid@durham.ac.uk

methods [6, 11, 4], Galerkin/least-squares methods [23, 4, 9] and Taylor-Galerkin methods [14, 8, 12]. However, it is well known that these schemes do not perform very satisfactory for transport problems with non-smooth solutions unless small time steps and highly refined grids are used in simulations. In case of three-dimensional problems as those considered in this study, these requirements are usually not feasible and may limit the performance of these Eulerian methods. The Lagrangian techniques are theoretically well suited for the numerical solution of transport problems due to the possibility for using large time steps in the simulations. In practice, the computational mesh for the Lagrangian methods moves along the fluid particle trajectory which may yield to mesh distortion after a few time steps. Thus, because of this drawback, the Lagrangian methods are not recommended for the numerical solution of complex transport problems. In the semi-Lagrangian methods known also by modified method of characteristics, the computational mesh is taken to be fixed to overcome the drawback of the Lagrangian approach while keeping the advantage of the Lagrangian tracking algorithm along the characteristic curves. The main advantage of the modified method of characteristics lies on the fact that the Courant-Friedrichs-Lewy (CFL) condition is highly relaxed compared to the its Eulerian counterparts, see for example [17, 16]. In addition, the Lagrangian treatment in the modified method of characteristics greatly reduces the time truncation errors in the Eulerian methods, see [31, 38, 37, 16, 34] among others. Thus, the modified method of characteristics has the potential to be more suitable than Eulerian and Lagrangian methods for three-dimensional transport problems on unstructured tetrahedral meshes.

For two-dimensional problems, the modified method of characteristics appears in the literature in several forms, see for instance [32, 10, 25, 3]. The method has also been studied for three-dimensional transport problems in [25, 3]. In finite element framework, analysis of convergence and stability of the modified method of characteristics have been carried out in many studies, see for example [15, 30, 16]. It should be stressed that the central idea in the modified method of characteristics is to rewrite the governing equations in terms of Lagrangian coordinates as defined by the characteristics associated with the transport problem under consideration. The time derivative and the advection terms are combined as a directional derivative along the characteristic curves leading to a characteristic time-stepping procedure. This type of numerical methods allows for time steps that exceed those permitted by the CFL stability condition in the Eulerian-based methods for convection-dominated problems. A class of modified methods of characteristics has been investigated in [15, 30, 19, 18, 17] for two-dimensional problems and in [13, 26, 29, 41, 21] for transport problem in three space dimensions. However, the results reported in these references either consider linear three-dimensional problems with constant velocity fields or employ structured meshes for the spatial discretization. It should be noted that tetrahedral finite elements are very attractive in numerical simulations because of their flexibility for representing irregular boundaries and for local mesh refinements. In addition, solving transport problems subject to sharp gradients in three space dimensions is still a challenge for many finite element discretizations including the semi-Lagrangian methods. Applied to these problems, the numerical solution obtained using the conventional modified method of characteristics either develops spurious oscillations or it is affected by a large artificial viscosity. Spurious oscillations and artificial viscosity often deteriorate the accuracy of the solution, so the numerical solution may become physically unacceptable, see [20, 28] for examples in two space dimensions. For two-dimensional problems in structured grids, a class of conservative quasi-monotone semi-Lagrangian methods has been proposed in [2, 20, 33] to overcome these difficulties. In the current work, a procedure using three-dimensional slope limiters is developed to eliminate the principal drawback of the conventional modified method of characteristics, which is the failure to preserve monotonicity. In a semi-Lagrangian framework, the key idea of the slope-limiting procedure consists in writing the local solution as a convex combination of lower and higher order interpolations. This allows to convert the method to non-oscillatory and monotonicity-preserving at minor additional computational cost. Here, the higher and lower interpolation solutions use two different basis functions of higher and lower order, respectively. Similar techniques but based on flux-corrector procedures have been used for solving advection problems using the Eulerian methods in [27, 35].

This paper proposes a class of slope limiters for the numerical solution of three-dimensional transport problems using the modified method of characteristics on unstructured finite element meshes. The presented results show that the proposed method is monotone for transport problems with steep gradients. Moreover, it requires significantly less time steps than classical explicit Eulerian finite element methods. This can be a major advantage when modelling transport problems for industrial applications where steep discontinuities and steep gradients may pose a significant challenge in terms of required CFL conditions. To our knowledge, this is the first time that three-dimensional transport problems are numerically solved using a monotonicity-preserving modified method of characteristics on unstructured tetrahedral meshes. To demonstrate the basic algorithms and show that it can adapt to three-dimensional features of a solution, we have implemented a slope limiter procedure to solve passive transport problems in three-dimensional flow fields. The rest of the paper is organized as follows. Formulation of slope limiters in the modified method of characteristics for three-dimensional transport problems is presented in section 2. This section includes the calculation of departures points and the implementation of slopes limiters on unstructured tetrahedral meshes. In section 3, we examine the numerical performance of the proposed method using several test examples of convection problems in three-dimensional domains. The proposed method is shown to enjoy the expected accuracy as well as the monotonicity. Concluding remarks are given in section 4.

2 Slope limiters for modified method of characteristics

To describe the formulation of the modified method of characteristics in tetrahedral finite element framework, we consider the following three-dimensional transport problem

$$\begin{aligned} \frac{Dc}{Dt} := \frac{\partial c}{\partial t} + \mathbf{v}(\mathbf{x},t)\cdot\nabla c &= 0, \qquad (\mathbf{x},t)\in\Omega\times(0,T], \\ c(\mathbf{x},0) &= c_0(\mathbf{x}), \qquad \mathbf{x}\in\Omega, \end{aligned} \tag{1}$$

where $\mathbf{x}=(x,y,z)^T$ is the position variable, $\nabla=\left(\frac{\partial}{\partial x},\frac{\partial}{\partial y},\frac{\partial}{\partial z}\right)^T$ the gradient vector, Ω a spacial bounded domain in $\mathbb{R}^3$ with boundary $\partial\Omega$, and $(0,T]$ a time interval. Here, $c(\mathbf{x},t)$ denotes the concentration of some transported species, $u_0(\mathbf{x})$ the initial concentration, and $\mathbf{v}(\mathbf{x},t)=(v_1(\mathbf{x},t),v_2(\mathbf{x},t),v_3(\mathbf{x},t))^T$ the velocity field assumed to be given either by measurements or by solving a flow problem such as Navier-Stokes or shallow water equations. In (1), the transport equation has to be solved for the time interval $(0,T]$ in the spatial domain Ω equipped with given boundary and initial conditions. In practice, the boundary conditions are problem-dependent and their discussion is postponed for section 3 where numerical examples are discussed in details. Note that the total derivative in (1) measures the rate of change of the function c following the trajectories of the flow particles.

To discretize the three-dimensional spatial domain Ω, we generate a quasi-uniform partition $\Omega_h\subset\Omega$ of small finite elements $\mathcal{T}_j$ that satisfy the following conditions:

(i) $\Omega_h=\displaystyle\bigcup_{j=1}^{Ne}\mathcal{T}_j$, where Ne is the number of elements in Ω_h.

(ii) If $\mathcal{T}_i$ and $\mathcal{T}_j$ are two different elements of Ω_h, then

$$\mathcal{T}_i\cap\mathcal{T}_j=\begin{cases} P_{ij}, & \text{a mesh point, or}\\ \Gamma_{ij}, & \text{a common face, or}\\ \partial\Gamma_{ij}, & \text{a common edge, or}\\ \emptyset, & \text{empty set.}\end{cases}$$

(iii) There exists a positive constant k such that for all $j \in \{1, \cdots, Ne\}$, $\frac{R_j}{h_j} > k$ $(h_j \leq h)$, where R_j is the radius of the sphere inscribed in $\mathcal{T}_j$ and h_j is the largest edge of $\mathcal{T}_j$.

The conforming finite element space for the solution that we use is defined as

$$V_h = \Big\{ c_h \in \mathcal{C}^0(\Omega) : \quad c_h\big|_{\mathcal{T}_j} \in P(\mathcal{T}_j), \quad \forall\, \mathcal{T}_j \in \Omega_h \Big\}, \tag{2}$$

with

$$P(\mathcal{T}_j) = \Big\{ p(\mathbf{x}) : \quad p(\mathbf{x}) = \hat{p} \circ F_j^{-1}(\mathbf{x}), \quad \hat{p} \in P_m(\hat{\mathcal{T}}) \Big\},$$

where $\hat{p}(\mathbf{x})$ is a polynomial of degree $\leq m$ defined on the element $\hat{\mathcal{T}}_j$ and $P_m(\hat{\mathcal{T}})$ is the set of polynomials of degree $\leq m$ defined on the reference element $\hat{\mathcal{T}}$. Here $F_j : \hat{\mathcal{T}} \longrightarrow \mathcal{T}_j$ is an invertible one-to-one mapping between physical and reference elements.

For the time discretization, we divide the time interval into N subintervals $[t_n, t_{n+1}]$ with length $\Delta t = t_{n+1} - t_n$ for $n = 0, 1, \ldots, N$. We also use the notation w^n to denote the value of a generic function w at time t_n. Hence, we formulate the finite element solution to $w^n(\mathbf{x})$ as

$$w_h^n(\mathbf{x}) = \sum_{j=1}^{M} W_j^n \phi_j(\mathbf{x}), \tag{3}$$

where M is the number of solution mesh points in the partition Ω_h. The functions W_j^n are the corresponding nodal values of $w_h^n(\mathbf{x})$ defined as $W_j^n = w_h^n(\mathbf{x}_j)$ where $\{\mathbf{x}_j\}_{j=1}^M$ are the set of solution mesh points in the partition Ω_h. In (3), $\{\phi_j\}_{j=1}^M$ are the set of global nodal basis functions of V_h characterized by the property $\phi_i(\mathbf{x}_j) = \delta_{ij}$ with δ_{ij} denoting the Kronecker symbol. We introduce $\{\mathbf{x}_1, \ldots, \mathbf{x}_{Nd}\}$ the set of Nd node points in the element $\mathcal{T}_j$. Hereafter, unless otherwise stated, the subscripts h and j are used to refer to coefficients associated with the whole mesh Ω_h and a mesh element $\mathcal{T}_j$, respectively.

2.1 Calculation of departure points

Let us denote by $\mathbf{X}_h(t)$ the discrete characteristic curves associated with the material derivative (1) which solve the following initial-value problem

$$\begin{aligned} \frac{d\mathbf{X}_h(t)}{dt} &= \mathbf{v}_h\left(\mathbf{X}_h(t), t\right), \quad \forall\, (\mathbf{x}_h, t) \in \Omega_h \times [t_n, t_{n+1}], \\ \mathbf{X}_h(t_{n+1}) &= \mathbf{x}_h, \end{aligned} \tag{4}$$

with $\mathbf{X}_h(t) = \left(X_h(t), Y_h(t), Z_h(t)\right)^T$ is the departure point representing the location at time t of a particle that reaches the point $\mathbf{x}_h = (x_h, y_h, z_h)^T$ at time t_{n+1}. Thus, for all $\mathbf{x}_h \in \Omega_h$ and $t \in [t_n, t_{n+1}]$ the solution of (4) can be expressed as

$$\mathbf{X}_h(t_n) = \mathbf{x}_h - \int_{t_n}^{t_{n+1}} \mathbf{v}\left(\mathbf{X}_h(t), t\right)\, dt. \tag{5}$$

In order to approximate the integral in (5), we use a second-order extrapolation based on the mid-point rule as proposed in [37] in the context of semi-Lagrangian schemes to integrate the weather prediction equations. Hence, we use $\mathbf{d}_h$ to denote the displacement between a mesh point on the new level, $\mathbf{x}_h$, and the departure point of the trajectory to this point on the previous time level $\mathbf{X}_h(t_n)$, *i.e.*

$$\mathbf{d}_h = \mathbf{x}_h - \mathbf{X}_h(t_n).$$

Applying the mid-point rule to approximate the integral in (5) yields

$$\mathbf{d}_h = \Delta t \mathbf{v}_h \left(\mathbf{X}_h(t_{n+\frac{1}{2}}), t_{n+\frac{1}{2}} \right). \tag{6}$$

Using the second-order extrapolation

$$\mathbf{v}_h(\mathbf{x}_h, t_{n+\frac{1}{2}}) = \frac{3}{2}\mathbf{v}_h(\mathbf{x}_h, t_n) - \frac{1}{2}\mathbf{v}_h(\mathbf{x}_h, t_{n-1}), \tag{7}$$

and the second-order approximation

$$\mathbf{X}_h(t_{n+\frac{1}{2}}) = \mathbf{x}_h - \frac{1}{2}\mathbf{d}_h,$$

we obtain the following implicit formula for $\mathbf{d}_h$

$$\mathbf{d}_h = \Delta t \left(\frac{3}{2}\mathbf{v}_h \left(\mathbf{x}_h - \frac{1}{2}\mathbf{d}_h, t_n \right) - \frac{1}{2}\mathbf{v}_h \left(\mathbf{x}_h - \frac{1}{2}\mathbf{d}_h, t_{n-1} \right) \right).$$

To compute $\mathbf{d}_h$ we consider the following successive iteration procedure:

$$\begin{aligned} \mathbf{d}_h^{(0)} &= \Delta t \left(\frac{3}{2}\mathbf{v}_h \left(\mathbf{x}_h, t_n \right) - \frac{1}{2}\mathbf{v}_h \left(\mathbf{x}_h, t_{n-1} \right) \right), \\ \mathbf{d}_h^{(k)} &= \Delta t \left(\frac{3}{2}\mathbf{v}_h \left(\mathbf{x}_h - \frac{1}{2}\mathbf{d}_h^{(k-1)}, t_n \right) - \frac{1}{2}\mathbf{v}_h \left(\mathbf{x}_h - \frac{1}{2}\mathbf{d}_h^{(k-1)}, t_{n-1} \right) \right), \quad k = 1, 2, \ldots. \end{aligned} \tag{8}$$

The iterations (8) are terminated when the following criteria

$$\frac{\left\| \mathbf{d}^{(k)} - \mathbf{d}^{(k-1)} \right\|}{\left\| \mathbf{d}^{(k-1)} \right\|} < \varepsilon, \tag{9}$$

is satisfied for the Euclidean norm $\| \cdot \|$ and a given tolerance ε. In all our simulations, the iterations in (8) were continued until the trajectory changed by less than $\varepsilon = 10^{-7}$. However, in practice it is not recommended to repeat the iteration process more than a few times due to efficiency considerations.

Note that, since the departure point $\mathbf{X}_h(t)$ would not lie on a mesh point in Ω_h, the concentration at the characteristic feet must be obtained by interpolation from known values at the gridpoints of the element where $\mathbf{X}_h(t)$ belongs. Here, the Lagrangian interpolation is performed in the host element of departure points using the finite element basis functions. Therefore, an advantage of the finite element method is that it can employ a high-order basis functions and there is no need for constructing explicitly interpolation polynomials as usually carried out in the finite difference discretizations, compare the references [37, 33, 34] among others. Thus, the finite element solution $\widetilde{c}_h^n = c\left(\mathbf{X}_h(t), t_n\right)$ is approximated by

$$\widetilde{c}_h^n = \sum_{j=1}^{M} \widetilde{\mathcal{C}}_j^n \phi_j, \tag{10}$$

where $\widetilde{\mathcal{C}}_j^n$ are nodal solutions evaluated by finite element interpolation of $c_h^n(\mathbf{x})$ at the feet of characteristic curves $\mathbf{X}_h(t)$. This procedure needs less computational work than using a piecewise exact method for projecting the information from the background Eulerian grid onto the Lagrangian grid as reported in [15, 30] among others. Note that other interpolation procedures such as bi-cubic spline [1] can also be used in (10).

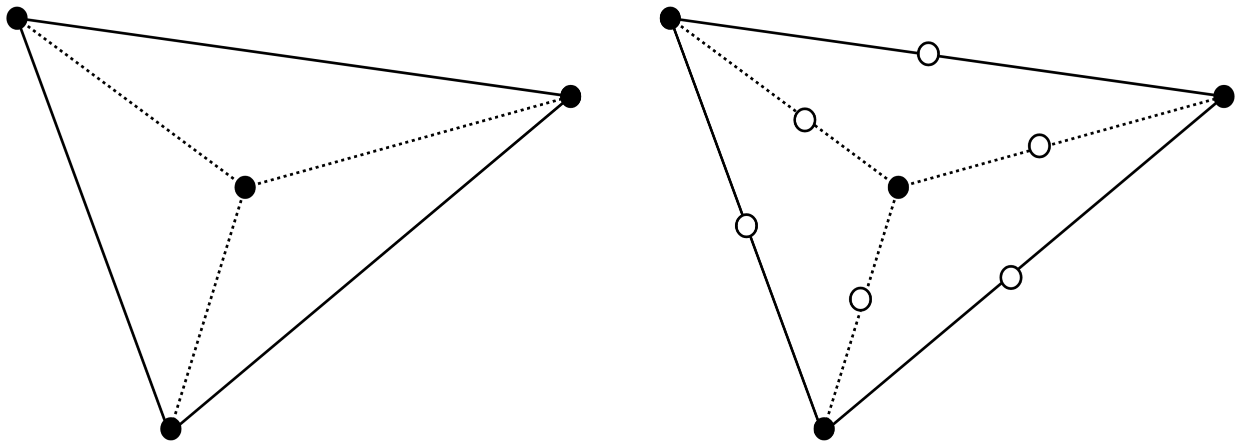

Figure 1: An example of low-order (left) and high-order (right) finite elements used in our simulations.

2.2 Formulation of slope limiters

The most common interpolation procedures in practical applications are the Lagrangian interpolations of high degrees. However, most of interpolation procedures of degree ≥ 2 are not monotone and do note conserve the positivity of the computed solutions. In order to overcome this drawback, we incorporate slope limiters to our modified method of characteristics. This implies that a solution, obtained by interpolating in a tetrahedral element, lies between the maximum and minimum values in the vertices of this grid element. In this way we obtain a non-oscillatory algorithm at minor additional computational cost that possesses good shape preserving of the transported fields in the vicinity of strong gradients and preserves the order of convergence in regions where the solution is sufficiently smooth. An example of low-order and high-order solution elements used in our computations is shown in Figure 1. Here, the linear P_1 elements and the quadratic P_2 elements are used as low-order and high-order interpolations, respectively.

Next, we formulate the resulting slope limiters for the convection problem (1) using the finite elements shown in Figure 1. Thus, the numerical procedure to approximate the solution $\widetilde{c}^n$ is carried out in the following steps:

1. Compute the departure point $\mathbf{X}_j(t_n)$ using the procedure (5)-(8).
2. Search-locate the tetrahedral element $\widetilde{\mathcal{T}}_j$ where the departure point $\mathbf{X}_j(t_n)$ belongs.
3. Calculate the high-order nodal approximation
$$\widetilde{c}^n_{Hj} = \sum_{k=1}^{N_H} \widetilde{C}_{jk} \phi_{jk} \left(\mathbf{X}_j(t_n)\right), \tag{11}$$
where $\{\phi_{j1}, \ldots, \phi_{jN_H}\}$ are the quadratic local basis functions of the element $\widetilde{\mathcal{T}}_j$. As stated before, Lagrange interpolations of degree ≥ 2 lead to numerical results that exhibit an oscillatory behavior and do not satisfy the discrete maximum principle.
4. Calculate the low-order nodal approximation
$$\widetilde{c}^n_{Lj} = \sum_{k=1}^{N_L} \widetilde{C}_{jk} \varphi_{jk} \left(\mathbf{X}_j(t_n)\right), \tag{12}$$

where $\{\varphi_{j1}, \ldots, \varphi_{jN_L}\}$ are the linear local basis functions on the element $\widetilde{\mathcal{T}}_j$. It is well-known that the linear interpolation is monotone and the numerical solutions obtained by this linear interpolation are free of oscillations and artificial extrema.

5. Evaluate the solution $\widetilde{c}_j^n$ using the combination

$$\widetilde{c}_j^n = \Psi_j^n \widetilde{c}_{Hj}^n + \left(1 - \Psi_j^n\right) \widetilde{c}_{Lj}^n, \tag{13}$$

where $\Psi_j^n \in [0,1]$ is a limiting function used to control the amount of correction in the low-order approximation (12) in order to obtain a non-oscillatory solution. Note that for $\Psi_j^n = 0$, the obtained solution in (13) reduces to the linear approximation, whereas a quadratic approximation is achieved for $\Psi_j^n = 1$. In the current study, to improve the accuracy and reduce the numerical diffusion for the low order interpolation, we consider a limiter function Ψ_j^n based on the slope of the solution

$$\sigma_j^n = \max\left(c_j^+ - \widetilde{c}_j^n, \widetilde{c}_j^n - c_j^-\right)$$

where c_j^+ and c_j^- are respectively, the maximum and minimum of the nodal solutions c_{ji}^n (with $i = 1, \ldots, N_H$) at the host element $\widetilde{\mathcal{T}}_j$ defined as

$$c_j^- = \min\left(c_{j1}^n, \ldots, c_{jN_H}^n\right), \qquad c_j^+ = \max\left(c_{j1}^n, \ldots, c_{jN_H}^n\right).$$

Here, the limiter function Ψ_j^n should be selected to guaranty the monotonicity of the proposed modified method of characteristics *i.e.* the obtained solution $\widetilde{c}_j^n$ remains bounded in $[c_j^-, c_j^+]$ at each time step. In this study, we consider the following limiter function

$$\Psi_j^n = \begin{cases} \min\left(1, \max\left(\dfrac{c_j^+ - \widetilde{c}_{Lj}^n}{\widetilde{c}_{Hj}^n - \widetilde{c}_{Lj}^n}, \dfrac{c_j^- - \widetilde{c}_{Lj}^n}{\widetilde{c}_{Hj}^n - \widetilde{c}_{Lj}^n}\right)\right), & \text{if} \quad \widetilde{c}_{Hj}^n - \widetilde{c}_{Lj}^n \neq 0, \\ 1, & \text{if} \quad \widetilde{c}_{Hj}^n - \widetilde{c}_{Lj}^n = 0, \end{cases} \tag{14}$$

Note that this technique consists of computing the nodal values of the numerical solution by adding to the values of a low-order solution, which is monotone, a correction term that contains the contribution of a high-order solution and does not violate the monotonicity properties of the low-order solution. Indeed, using the limiting procedure (11)-(14), the computed solution remains within the largest and the smallest values of the solution in a set of mesh points surrounding the departure point. Therefore, the interpolation procedure does not generate any extrema which is not possessed by the solution in a neighborhood of the foot of characteristics. Note that other limiter functions can also be used in (13) without major conceptual modifications. For the mesh elements shown in Figure 1, the numbers of low-order and high-order local basis functions are $N_L = 4$ and $N_H = 10$, respectively.

3 Numerical results

To assess the performance of the proposed slope limiter procedure we present numerical results for several examples of transport problems in three space dimensions. For the first class of examples, analytical solutions are readily available which makes it ideal for a quantitative as well as qualitative validation of the proposed method. Thus, we can evaluate the total error as

$$E_{Tot} = \int_\Omega \left(c - c_{\text{exact}}\right)^2 \, d\mathbf{x},$$

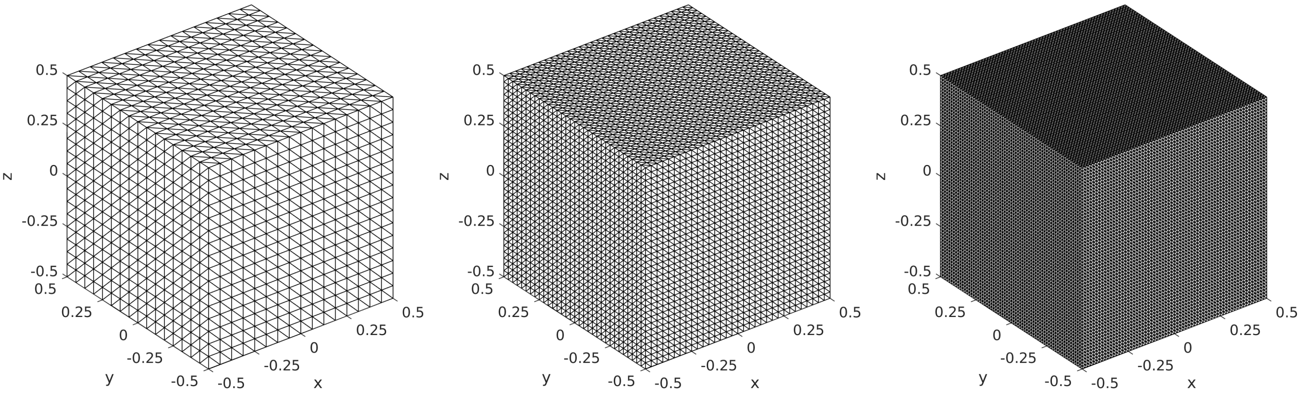

Figure 2: Finite element meshes with spatial steps $h = \frac{1}{32}$ (left), $\frac{1}{64}$ (middle) and $\frac{1}{128}$ (right) used in our simulations for transport problems in the circular and elliptical flow fields.

where c and c_{exact} are numerical solution and the analytical solution, respectively. We also compute the dissipation error E_{Diss} and the dispersion error E_{Disp} defined in [36] by

$$E_{Diss} = \left(\sigma\left(c\right) - \sigma\left(c_{\text{exact}}\right)\right)^2 + \left(\overline{c} - \overline{c}_{\text{exact}}\right)^2, \qquad E_{Disp} = 2\left(1-\rho\right)\sigma\left(c\right)\sigma\left(c_{\text{exact}}\right), \tag{15}$$

where $\sigma\left(c\right)$ and $\overline{c}$ are the canonical deviation and the mean of the solution c, respectively. In (15), ρ denotes the correlation coefficient between c and c_{exact}. It is also shown in [36] that

$$E_{Tot} = E_{Diss} + E_{Disp}.$$

In this section, we compare numerical results obtained using the linear P_1 elements, the quadratic P_2 elements and the proposed slope limiter procedure for the considered examples. We also present numerical results for a passive transport problem in a deformed pipeline with a well-defined flow field. It should be noted that we consider only problems with non-smooth solutions as for the case with smooth solutions, the limiting procedure introduces some peak clipping which is expected and it does not harm the overall accuracy of the method. For all simulations, the CFL number associated to the equation (1) is defined as

$$\text{CFL} = \sqrt{\text{CFL}_x^2 + \text{CFL}_y^2 + \text{CFL}_z^2}, \tag{16}$$

where

$$\text{CFL}_x = \max_{x,y,z} |v_1| \frac{\Delta t}{h}, \qquad \text{CFL}_y = \max_{x,y,z} |v_2| \frac{\Delta t}{h}, \qquad \text{CFL}_z = \max_{x,y,z} |v_3| \frac{\Delta t}{h},$$

with h is the spatial step in the finite element discretization. Here, the CFL number is fixed and values of the time step Δt are obtained form (16). Note that to reduce the computational cost, the CFL numbers are chosen as large as possible which yield explicit Eulerian-based schemes noncompetitive. All the computations were performed on a Pentium PC with Intel Core i7-7700HQ of 8 GB of RAM and 8 GHz using serial Fortran compiler.

3.1 Rotating slotted sphere in a circular flow

To assess the performance of the proposed slope limiters we consider the problem of slotted sphere in a circular flow field. Here, we solve the transport equation (1) in the unit cube $\Omega = [-0.5, 0.5] \times [-0.5, 0.5] \times [-0.5, 0.5]$ subject to the flow field $\mathbf{v} = (-\omega y, \omega x, 0)^T$, with an angular velocity $\omega = 4$. The sphere is centered at $(-0.25, 0, 0)$ of radius 0.15 and height of 1 along with a slot in the xy-plane of width 0.06 and a length of 0.22. For this case, the total time required for one complete revolution is $\frac{\pi}{2}$. Note that this

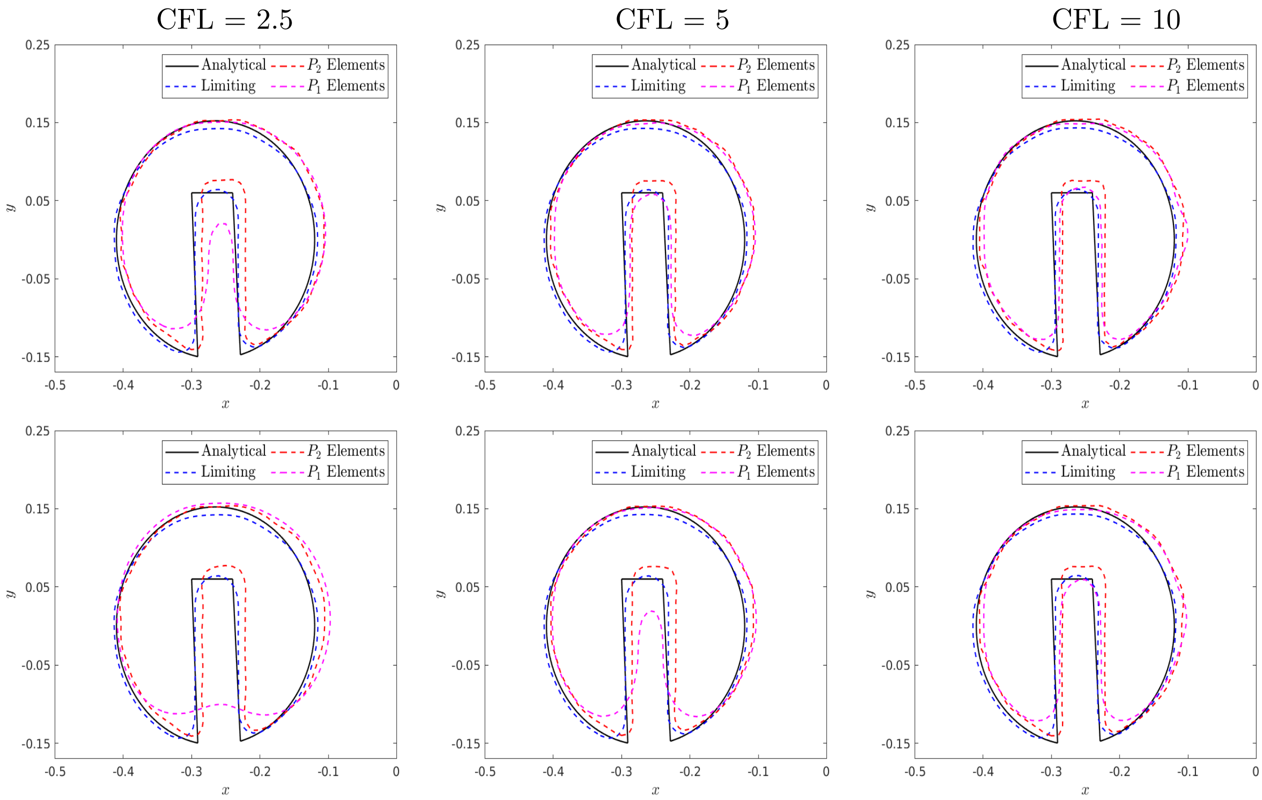

Figure 3: Contourlines of the solution at $z = 0$ for rotating slotted sphere in a circular flow after one revolution (first row) and after two revolutions (second row) using $h = \frac{1}{128}$ and different CFL numbers.

problem can be considered as an extension to three space dimensions of the well known two-dimensional Zalezak's slotted disk [40]. This class of test examples has been widely used to examine the non-oscillatory and monotonicity-preserving properties for numerical methods solving transport problems with sharp discontinuities. We present numerical results using three different structured meshes with $33 \times 33 \times 33$, $65 \times 65 \times 65$ and $129 \times 129 \times 129$ nodes as shown in Figure 2. Three different values for CFL are considered in this study namely CFL = 2.5, 5 and 10.

In Figure 3 we present contourlines in the xy-plane at $z = 0$ of the exact solution and the solutions obtained using the linear P_1 elements, the quadratic P_2 elements and the proposed slope limiter procedure after one and two revolutions on the mesh with $129 \times 129 \times 129$ nodes. For better insight, only part of the domain Ω, $[-0.5, 0] \times [-0.25, 0.25]$, is shown in these plots. Figure 4 illustrates the one-dimensional cross-sections at $y = z = 0$ of the results presented in Figure 3 using different number of elements and different values of CFL. Those one-dimensional cross-sections at $y = z = 0$ obtained after two revolutions are presented in Figure 5. A visual comparison of the computed results shows excessive numerical dissipation, severe overshoots, deformation and phase errors in the solutions computed using the linear P_1 elements and quadratic P_2 elements. After one complete revolution, the quadratic P_2 elements exhibit non-physical oscillations and substantially greater distortions localized specially at the feet and the upper face of the slotted sphere where discontinuities are more sharper than elsewhere in the computed solutions. The magnitude and frequency of these non-physical oscillations increase as the number of revolutions increases. On the other hand, numerical dissipation can be clearly seen in the results obtained using the linear P_1 elements. It is also noticeable that this numerical dissipation is more pronounced for small values of CFL and it reduces as the finite element mesh is refined. For example, in a mesh with $65 \times 65 \times 65$ nodes and after two revolutions, the solutions obtained using P_1 elements exhibit substantially large numerical diffusion at the feet of the slotted sphere where the gradient is sharp, see the results displayed in Figure 5. From the same figures we observe a full absence of

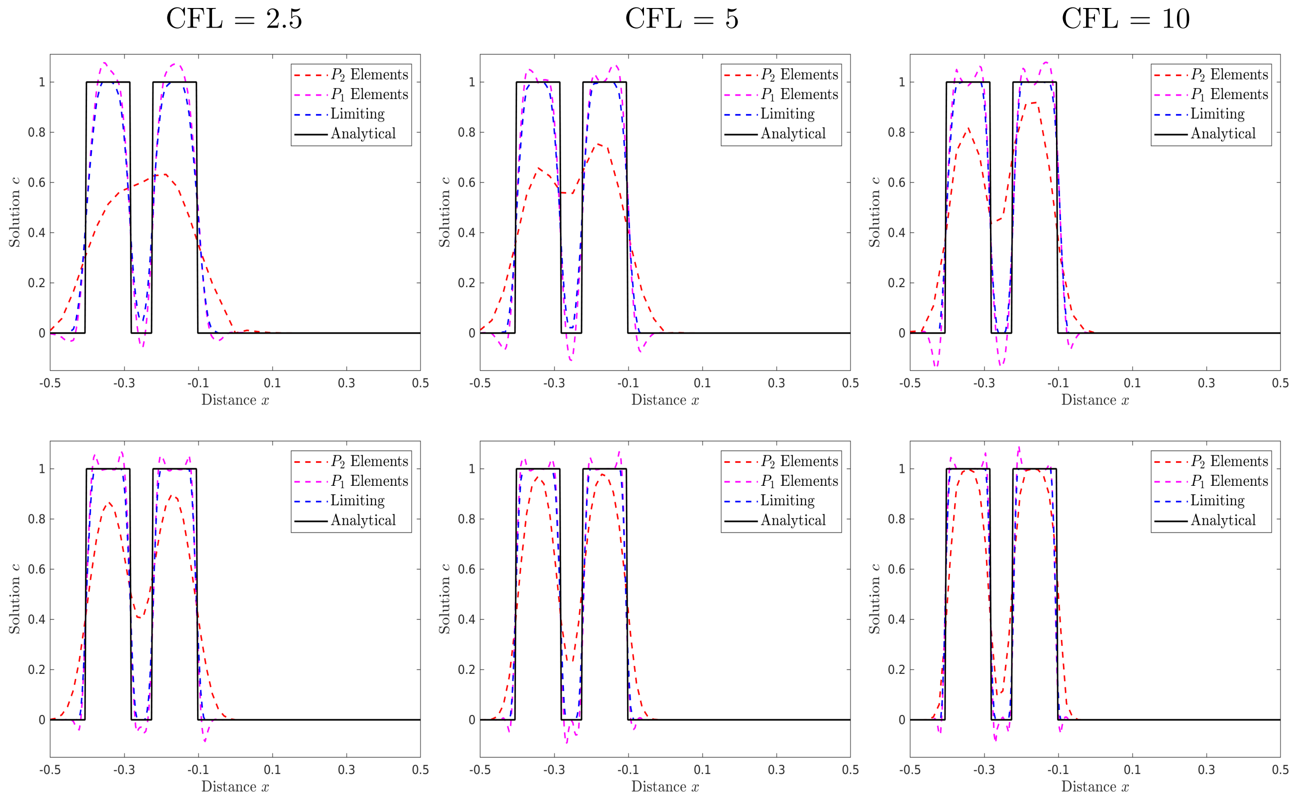

Figure 4: Cross-sections of the solution at $y = z = 0$ for rotating slotted sphere in a circular flow after 1 revolution using different values of CFL and meshes with $h = \frac{1}{64}$ (first row) and $h = \frac{1}{128}$ (second row).

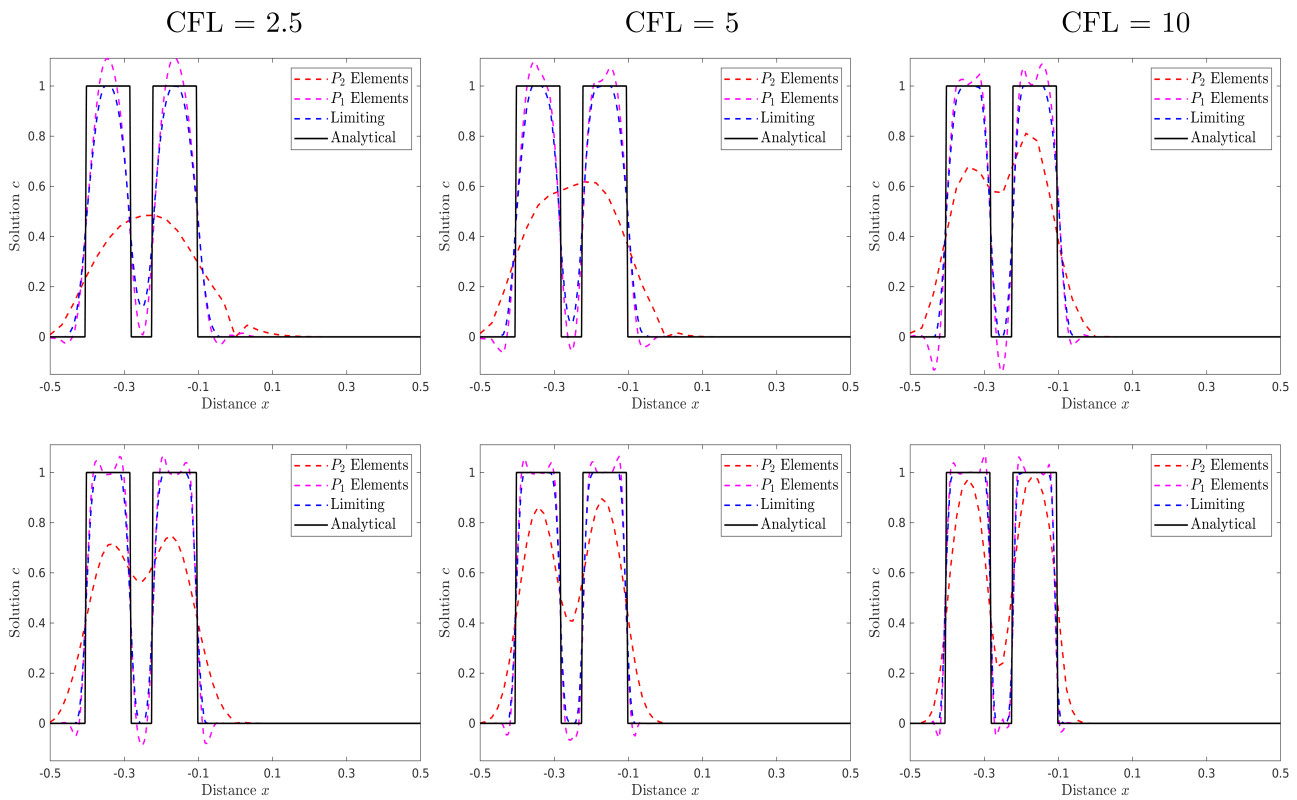

Figure 5: Same as Figure 4 but after two rotations.

these numerical dissipation and non-physical oscillations in the results obtained using our slope limiting procedure. Note that the accuracy in the proposed slope limiting procedure improves as the value of CFL increases, compare the results obtained using the low CFL = 2.5 and the high CFL = 10 in both Figure 4 and Figure 5. It is clear that the proposed finite element modified method of characteristics using slope limiters performs best for this test example.

A quantitative comparison study of the results obtained using the linear P_1 elements, the quadratic P_2 elements and the slope limiting approach for different values of CFL and mesh densities after one and two revolutions is summarized in Table 1. We report the minimum (Min) and the maximum (Max) values of the computed solutions, the errors E_{Diss}, E_{Disp} and E_{Tot} and the computational (CPU) times given in seconds. In terms of the considered errors in Table 1, the results obtained using the P_2 elements are more accurate than those obtained using the P_1 elements for all the considered values of CFL. It is also clear that the slope limiters do not deteriorate the accuracy of the proposed modified method of characteristics. Furthermore, increasing the values of CFL results in a decrease of the total error in all considered methods. Only results obtained using slope limiters exhibit a reduction of E_{Disp} errors as CFL increases. In addition, results obtained for E_{Diss}, E_{Disp} and E_{Tot} errors using the slope limiters in Table 1 demonstrate that these results are free from any spurious oscillations and monotone during the time integration process. In fact, the limited solutions reveal the physics well in this test example. From the values of Max and Min in Table 1 we observe very low values of Max for the results obtained using the P_1 elements and high and negative values for the results obtained using the P_2 elements which are avoided in the results obtained using the slope limiters. It is also evident that the CPU times in the modified method of characteristics using the P_2 elements are larger than the CPU times using the P_1 elements. For the considered transport conditions, the CPU time of the quadratic P_2 elements is about seven times larger than the CPU time of the linear P_1 elements. However, the difference between the CPU times for the quadratic P_2 elements and the slope limiters it minimal and it is about 1% for all the simulations.

3.2 Transport of a unit sphere in elliptical flows

In this example we consider a fully three-dimensional transport problem of rotating a pulse in oblique flow fields proposed in [7]. The governing equations are given by (1) where the velocity is defined as $\mathbf{v} = (-\omega y, \omega x, (x+y)/2)^T$ with $\omega = 4$. Initial and boundary conditions are derived from the analytical solution

$$u(x,y,z,t) = \begin{cases} 1, & \text{if} \quad r(t) < R, \\ \\ 0, & \text{if} \quad r(t) \geq R, \end{cases}$$

where $R = 0.1$ and $r(t) = \sqrt{(\bar{x}(t)-x_0)^2 + (\bar{y}(t)-y_0)^2 + (\bar{z}(t)-z_0)^2}$ with $x_0 = -0.25$, $y_0 = 0$, $z_0 = 0.25$, $\bar{x}(t) = x\cos(\omega t) + y\sin(\omega t)$, $\bar{y}(t) = -x\sin(\omega t) + y\cos(\omega t)$ and $\bar{z} = z - (\bar{x} - x + \bar{y} - y)/2$. As in the previous test example, the computational domain is the unit cube $\Omega = [-0.5, 0.5]^3$ covered by different uniform meshes with $33\times33\times33$, $65\times65\times65$ and $129\times129\times129$ nodes as shown in Figure 2. We also present numerical results using three different values for CFL = 2.5, 5 and 10. The time period required for one complete oblique rotation is $\frac{\pi}{2}$ and the time steps used in the simulations are calculated using the definition (16).

In Figure 6 we display the plots for iso-surface of the computed solutions after one rotation using two meshes with $65\times65\times65$ and $129\times129\times129$ nodes and CFL = 10. It is clear that the slope limiting procedure preserves the shape of the computed solutions with a little numerical diffusion compared to the solutions computed using the P_2 elements and the P_1 elements where oscillations are very remarkable. It is clear that the numerical results obtained using P_1 elements are more diffusive than those computed using the slope limiting procedure. To further visualize this effects, we display in Figure 7 and Figure

Table 1: Results for rotating slotted sphere in a circular flow. The analytical maximum and minimum are respectively Max=1.0 and Min=0.0.

		After 1 revolution						After 2 revolutions					
CFL	h	Min	Max	E_{Disp}	E_{Diss}	E_{Tot}	CPU	Min	Max	E_{Disp}	E_{Diss}	E_{Tot}	CPU
		P_1 Elements											
2.5	$\frac{1}{32}$	0.0000	0.3602	2.6719E-03	5.1444E-03	7.6371E-03	0.031	0.0000	0.1865	2.0509E-03	7.1030E-03	9.0219E-03	0.060
	$\frac{1}{64}$	0.0000	0.6320	3.2208E-03	2.1807E-03	5.1827E-03	0.238	0.0000	0.4849	3.0731E-03	3.2746E-03	6.1419E-03	0.472
	$\frac{1}{128}$	0.0000	0.8995	2.3714E-03	8.8907E-04	3.0242E-03	2.090	0.0000	0.7529	2.9597E-03	1.3736E-03	4.0975E-03	4.090
5	$\frac{1}{32}$	0.0000	0.5260	2.8787E-03	3.8512E-03	6.5355E-03	0.015	0.0000	0.3331	2.3931E-03	5.5839E-03	7.8179E-03	0.029
	$\frac{1}{64}$	0.0000	0.7556	3.0621E-03	1.4511E-03	4.2860E-03	0.125	0.0000	0.6186	3.3017E-03	2.1546E-03	5.2340E-03	0.266
	$\frac{1}{128}$	0.0000	0.9810	1.8323E-03	5.4500E-04	2.1421E-03	1.085	0.0000	0.8961	2.3656E-03	9.0983E-04	3.0402E-03	2.246
10	$\frac{1}{32}$	0.0000	0.6769	3.4328E-03	2.1178E-03	5.3078E-03	0.007	0.0000	0.5620	3.1676E-03	3.2698E-03	6.2186E-03	0.015
	$\frac{1}{64}$	0.0000	0.9190	2.6442E-03	8.6783E-04	3.2803E-03	0.070	0.0000	0.8114	3.1884E-03	1.2783E-03	4.2334E-03	0.129
	$\frac{1}{128}$	0.0000	0.9997	1.4669E-03	3.0690E-04	1.5384E-03	0.555	0.0000	0.9815	1.8234E-03	5.3752E-04	2.1258E-03	1.129
		P_2 Elements											
2.5	$\frac{1}{32}$	-0.1061	1.0218	3.2802E-03	7.8419E-04	3.8414E-03	0.268	-0.2098	0.9235	3.6790E-03	9.9452E-04	4.4600E-03	0.524
	$\frac{1}{64}$	-0.0901	1.1710	1.5634E-03	1.0687E-04	1.4408E-03	2.148	-0.0688	1.1814	1.7848E-03	1.6803E-04	1.7230E-03	4.151
	$\frac{1}{128}$	-0.1009	1.1603	9.7666E-04	4.0602E-05	7.8395E-04	17.070	-0.1229	1.1490	1.0882E-03	5.5210E-05	9.1033E-04	33.75
5	$\frac{1}{32}$	-0.1334	1.1267	2.9598E-03	4.3476E-04	3.1625E-03	0.139	-0.1015	1.0354	3.1999E-03	5.5963E-04	3.5214E-03	0.267
	$\frac{1}{64}$	-0.1563	1.1659	1.3537E-03	6.9264E-05	1.1957E-03	1.093	-0.1223	1.1501	1.5055E-03	1.1416E-04	1.3932E-03	2.162
	$\frac{1}{128}$	-0.1234	1.1626	8.9333E-04	2.8616E-05	6.8831E-04	9.044	-0.1035	1.1467	9.8127E-04	4.0370E-05	7.8811E-04	17.66
10	$\frac{1}{32}$	-0.1682	1.2132	3.0948E-03	2.1354E-04	3.0807E-03	0.068	-0.1549	1.2106	3.4200E-03	3.0723E-04	3.4956E-03	0.133
	$\frac{1}{64}$	-0.1640	1.2252	1.2831E-03	3.7750E-05	1.0930E-03	0.547	-0.2033	1.1797	1.3846E-03	6.3026E-05	1.2205E-03	1.108
	$\frac{1}{128}$	-0.1371	1.1808	8.3343E-04	1.7494E-05	6.1635E-04	4.500	-0.1545	1.1658	8.9279E-04	2.5524E-05	6.8370E-04	9.090
		Limiting Procedure											
2.5	$\frac{1}{32}$	0.0000	0.9256	3.3403E-03	7.4231E-04	3.8500E-03	0.300	0.0000	0.8404	3.6601E-03	9.5193E-04	4.3794E-03	0.594
	$\frac{1}{64}$	0.0000	1.0000	1.5824E-03	3.5808E-04	1.6897E-03	2.391	0.0000	1.0000	1.8189E-03	4.6818E-04	2.0340E-03	4.695
	$\frac{1}{128}$	0.0000	1.0000	9.9627E-04	8.3166E-05	8.4696E-04	19.73	0.0000	1.0000	1.1081E-03	1.1331E-04	9.8833E-04	38.59
5	$\frac{1}{32}$	0.0000	0.9874	2.9304E-03	4.9052E-04	3.1811E-03	0.162	0.0000	0.9190	3.2891E-03	5.8566E-04	3.6242E-03	0.303
	$\frac{1}{64}$	0.0000	1.0000	1.3792E-03	2.7710E-04	1.4080E-03	1.254	0.0000	1.0000	1.5391E-03	3.6819E-04	1.6577E-03	2.446
	$\frac{1}{128}$	0.0000	1.0000	9.0865E-04	5.7780E-05	7.3423E-04	10.10	0.0000	1.0000	1.0028E-03	8.0855E-05	8.5100E-04	20.10
10	$\frac{1}{32}$	0.0000	1.0000	2.7983E-03	3.3771E-04	2.9046E-03	0.076	0.0000	1.0000	3.2582E-03	4.1834E-04	3.4370E-03	0.153
	$\frac{1}{64}$	0.0000	1.0000	1.3118E-03	2.0057E-04	1.2639E-03	0.623	0.0000	1.0000	1.4054E-03	2.6965E-04	1.4264E-03	1.253
	$\frac{1}{128}$	0.0000	1.0000	8.4827E-04	3.9968E-05	6.5629E-04	5.188	0.0000	1.0000	9.1554E-04	5.7381E-05	7.4062E-04	10.42

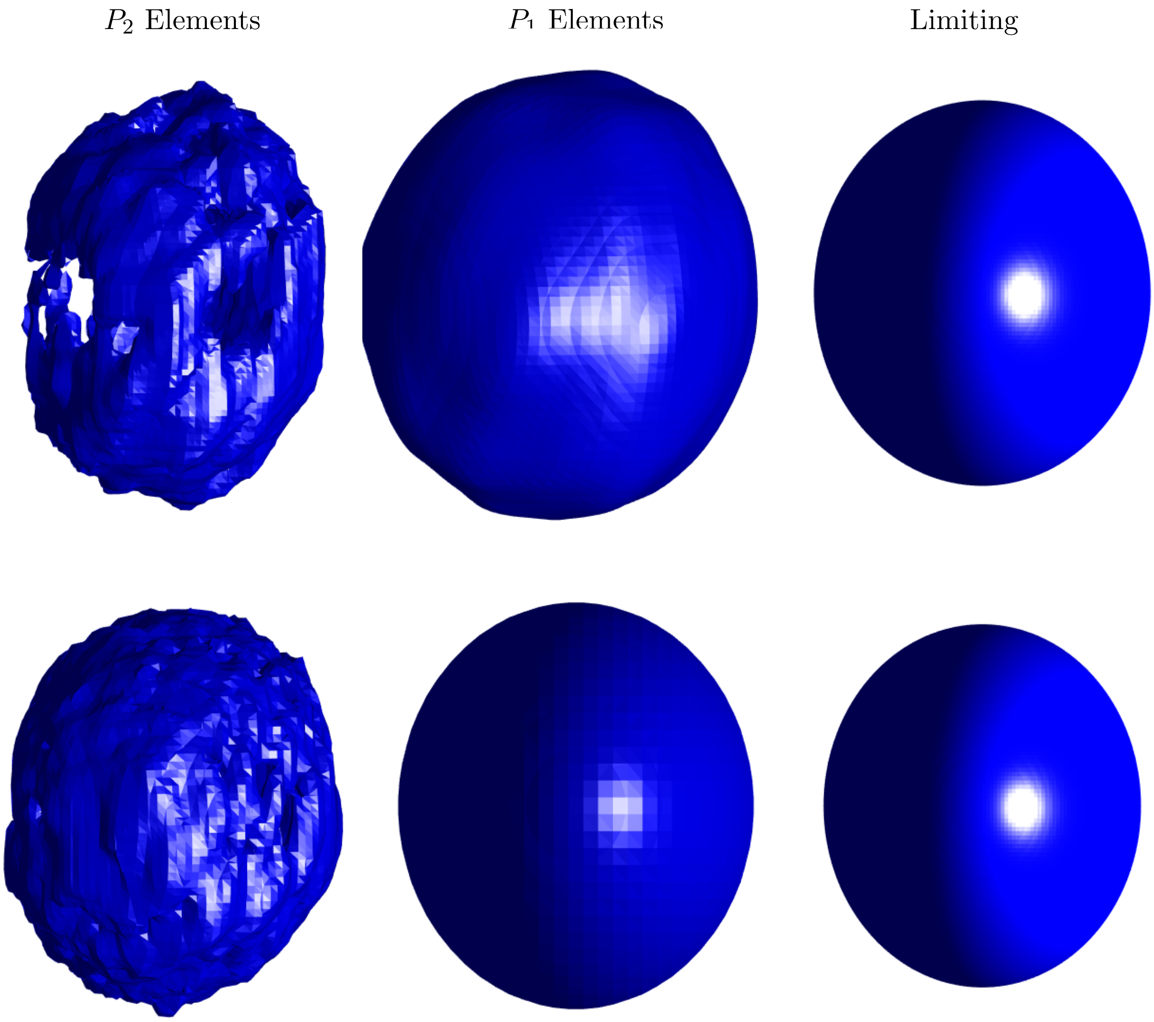

Figure 6: Iso-surfaces for rotating a sphere in the elliptical flow using CFL =10 and $h = \frac{1}{64}$ (first row) and $h = \frac{1}{128}$ (second row).

8 the one-dimensional cross-sections along the horizontal line at $y = z = 0$ for the results using three different values of CFL = 2.5, 5 and 10. As can be seen, the resolution and location of the transport in this example are deteriorated with the excessive numerical dissipation included by the P_1 elements. The solution obtained using the slope limiters eliminates the non-oscillatory oscillations near the feet of the sphere where discontinuities are steep. Note that, using slope limiters in the modified method of characteristics, the obtained solver is free of excessive numerical diffusion and non-physical oscillations. Thus, the transport is well resolved without requiring fine meshes or small time steps.

Now we turn our attention to a quantitative comparison of the results using the P_1 elements, P_2 elements and slope limiters for different values of CFL and mesh densities. In Table 2 we list the errors E_{Diss}, E_{Disp} and E_{Tot}, the maximum (Max) and the minimum (Min) values of the computed solutions and the CPU times for obtained using the considered methods after one and two revolutions. For this fully three-dimensional transport, the errors obtained using the proposed slope limiting and P_2 elements are more accurate than those results obtained using the P_1 elements for both one and two revolutions. Note that large errors and low values of Max in Table 2 for the results obtained using the P_1 elements. The unrealistic large values of Max in the results obtained using the P_2 elements are also noticeable in this table. Refining the mesh or increasing the value of CFL yield improvements in the results obtained

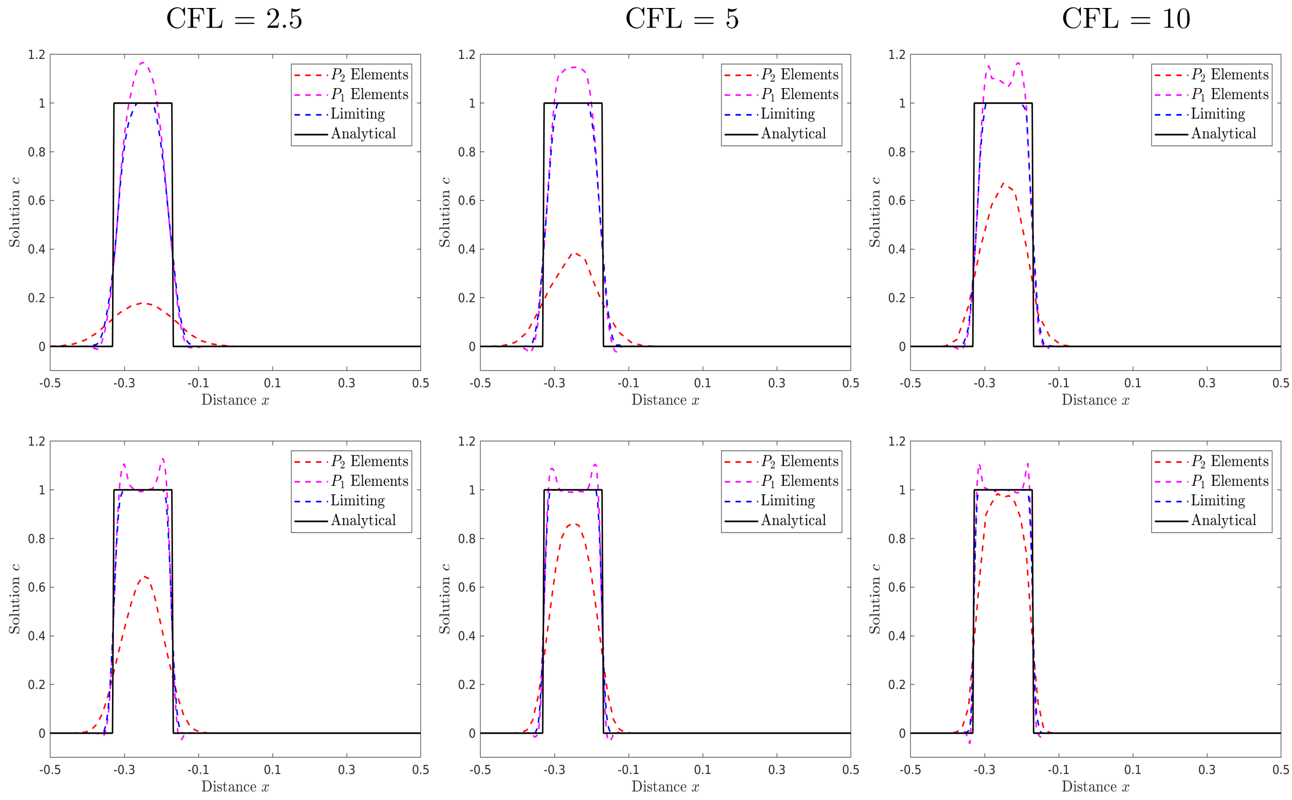

Figure 7: Cross-sections of the solution at $y = z = 0$ for rotating a sphere in the elliptical flow after one revolution using different CFL numbers and meshes with $h = \frac{1}{64}$ (first row) and $h = \frac{1}{128}$ (second row).

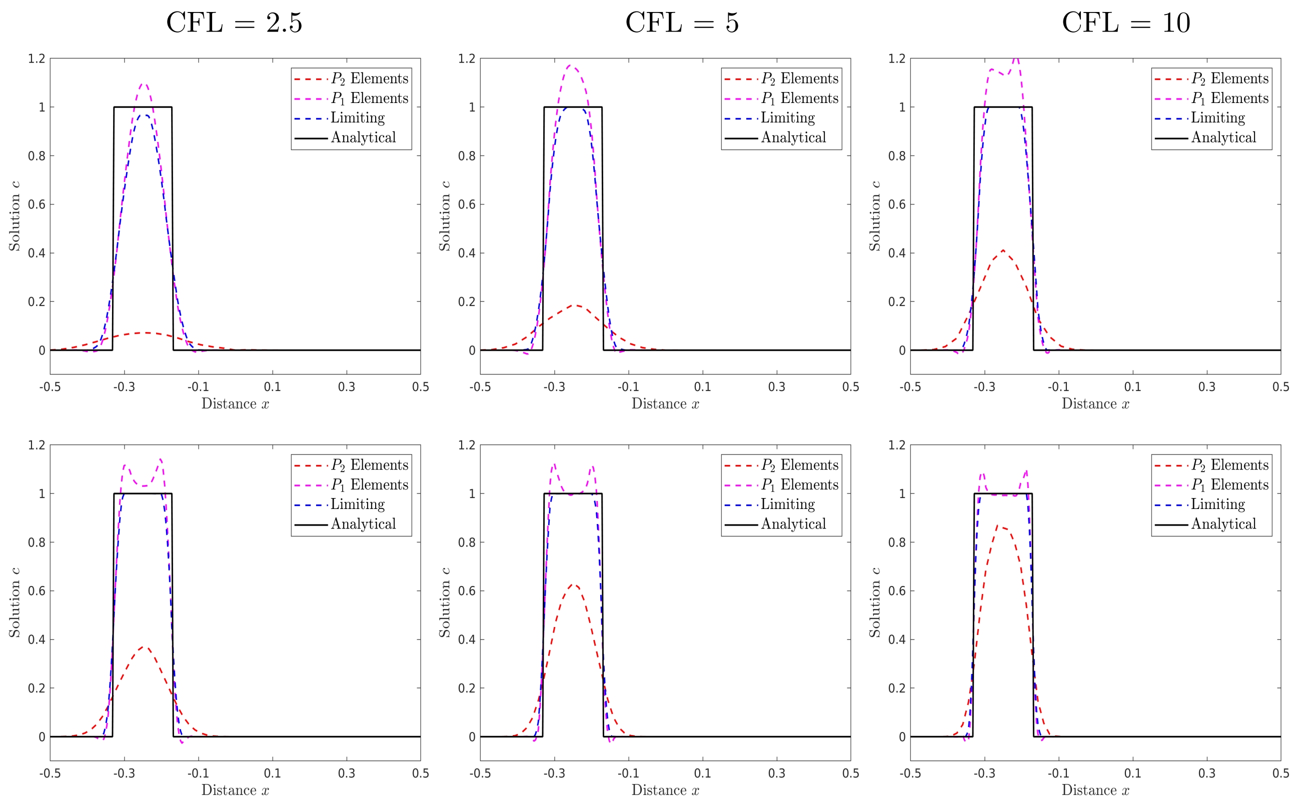

Figure 8: Same as Figure 7 but after two revolutions.

Table 2: Results for rotating a sphere in the elliptical flow. The analytical maximum and minimum are respectively Max = 1.0 and Min=0.0.

		After 1 revolution						After 2 revolutions					
CFL	h	Min	Max	E_{Disp}	E_{Diss}	E_{Tot}	CPU	Min	Max	E_{Disp}	E_{Diss}	E_{Tot}	CPU
		P_1 Elements											
2.5	$\frac{1}{32}$	0.0000	0.0161	1.5005E-04	1.9951E-03	2.1412E-03	0.031	0.0000	0.0041	7.0019E-05	2.1154E-03	2.1830E-03	0.061
	$\frac{1}{64}$	0.0000	0.1796	5.4135E-04	1.1768E-03	1.7081E-03	0.262	0.0000	0.0719	3.9357E-04	1.5624E-03	1.9477E-03	0.538
	$\frac{1}{128}$	0.0000	0.6464	4.7187E-04	5.2717E-04	9.8943E-04	2.161	0.0000	0.3700	5.0952E-04	8.5891E-04	1.3590E-03	4.336
5	$\frac{1}{32}$	0.0000	0.0537	2.6906E-04	1.7682E-03	2.0315E-03	0.015	0.0000	0.0165	1.4659E-04	1.9995E-03	2.1423E-03	0.030
	$\frac{1}{64}$	0.0000	0.3887	5.6624E-04	8.0531E-04	1.3611E-03	0.131	0.0000	0.1873	5.1071E-04	1.2050E-03	1.7062E-03	0.263
	$\frac{1}{128}$	0.0000	0.8636	4.0305E-04	2.8781E-04	6.8127E-04	1.178	0.0000	0.6315	4.6661E-04	5.3054E-04	9.8758E-04	2.379
10	$\frac{1}{32}$	0.0000	0.1908	3.9405E-04	1.3819E-03	1.7684E-03	0.007	0.0000	0.0622	2.8122E-04	1.7467E-03	2.0222E-03	0.016
	$\frac{1}{64}$	0.0000	0.6702	5.2616E-04	4.5062E-04	9.6602E-04	0.072	0.0000	0.4120	5.6802E-04	7.6675E-04	1.3242E-03	0.141
	$\frac{1}{128}$	0.0000	0.9875	3.4511E-04	1.4188E-04	4.7734E-04	0.669	0.0000	0.8688	4.0575E-04	2.8169E-04	6.7778E-04	1.330
		P_2 Elements											
2.5	$\frac{1}{32}$	-0.0266	0.6240	7.7153E-04	3.5592E-04	1.1152E-03	0.282	-0.0199	0.4090	7.8535E-04	6.0656E-04	1.3802E-03	0.555
	$\frac{1}{64}$	-0.0476	1.1667	3.7805E-04	1.0765E-04	4.7677E-04	2.295	-0.0499	1.0984	4.3900E-04	1.6810E-04	5.9812E-04	4.471
	$\frac{1}{128}$	-0.0630	1.1525	2.1812E-04	1.9532E-05	2.2869E-04	20.04	-0.0545	1.1709	2.5513E-04	2.7062E-05	2.7324E-04	40.47
5	$\frac{1}{32}$	-0.0405	0.9120	6.7413E-04	1.5718E-04	8.1934E-04	0.141	-0.0317	0.6985	7.6562E-04	2.8457E-04	1.0379E-03	0.279
	$\frac{1}{64}$	-0.0741	1.1732	3.4061E-04	5.7453E-05	3.8889E-04	1.172	-0.0471	1.1634	3.8537E-04	9.0711E-05	4.6694E-04	2.327
	$\frac{1}{128}$	-0.0693	1.1498	1.8736E-04	1.4812E-05	1.9322E-04	10.97	-0.0528	1.1534	2.1960E-04	2.1176E-05	2.3183E-04	22.24
10	$\frac{1}{32}$	-0.0633	1.0833	6.1632E-04	6.3603E-05	6.6815E-04	0.073	-0.0732	0.9429	7.1400E-04	1.3599E-04	8.3746E-04	0.147
	$\frac{1}{64}$	-0.0851	1.1952	2.9913E-04	3.9644E-05	3.2975E-04	0.624	-0.0695	1.2141	3.3638E-04	5.6533E-05	3.8391E-04	1.242
	$\frac{1}{128}$	-0.1064	1.1445	1.5785E-04	1.0458E-05	1.5935E-04	6.409	-0.0746	1.1307	1.8578E-04	1.5113E-05	1.9196E-04	12.887
		Limiting Procedure											
2.5	$\frac{1}{32}$	0.0000	0.5447	7.9129E-04	4.1905E-04	1.1962E-03	0.318	0.0000	0.3640	8.1227E-04	6.4459E-04	1.4431E-03	0.626
	$\frac{1}{64}$	0.0000	1.0000	3.9685E-04	1.4018E-04	5.2679E-04	2.555	0.0000	0.9658	4.7262E-04	1.9611E-04	6.5808E-04	5.066
	$\frac{1}{128}$	0.0000	1.0000	2.2318E-04	3.9724E-05	2.5355E-04	22.69	0.0000	1.0000	2.6002E-04	5.4706E-05	3.0524E-04	44.82
5	$\frac{1}{32}$	0.0000	0.8031	7.0244E-04	1.9823E-04	8.8656E-04	0.158	0.0000	0.6266	8.0508E-04	3.1540E-04	1.1057E-03	0.320
	$\frac{1}{64}$	0.0000	1.0000	3.4284E-04	9.0686E-05	4.2347E-04	1.386	0.0000	1.0000	4.0038E-04	1.2699E-04	5.1701E-04	2.635
	$\frac{1}{128}$	0.0000	1.0000	1.9094E-04	2.9705E-05	2.1142E-04	12.28	0.0000	1.0000	2.2327E-04	4.2250E-05	2.5624E-04	24.59
10	$\frac{1}{32}$	0.0000	0.9197	6.1446E-04	1.2010E-04	7.2125E-04	0.066	0.0000	0.8172	7.2177E-04	1.9790E-04	9.0515E-04	0.163
	$\frac{1}{64}$	-0.0000	1.0000	2.9581E-04	6.8055E-05	3.5412E-04	0.712	0.0000	1.0000	3.4286E-04	9.2214E-05	4.2508E-04	1.414
	$\frac{1}{128}$	0.0000	1.0000	1.6095E-04	1.9777E-05	1.7153E-04	7.159	0.0000	1.0000	1.9016E-04	2.9053E-05	2.0997E-04	14.09

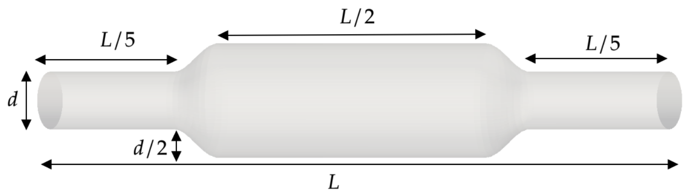

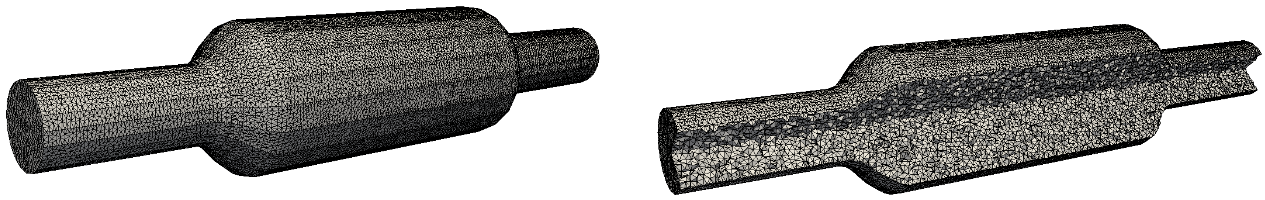

Figure 10: Computational mesh used for passive transport in a deformed pipe.

for the errors and the maximum values of the computed solutions in all methods but the results obtained using the proposed slope limiting are more accurate than those obtained using the P_1 and P_2 elements. Needless to mention that, as in the previous test example, the additional computational work required for the slope limiting procedure has been kept minimal compared to the its counterpart using the P_2 elements, see the differences in CPU times in Table 2. Therefore, the performance of our modified method of characteristics is very attractive since the computed solutions remain monotone and highly accurate without requiring highly refined meshes or small time steps to be accounted for in the simulations.

3.3 Passive transport in a deformed pipe

Our final concern is to ascertain the performance of the proposed modified method of characteristics for solving transport problems in pipeline flows. To this end we consider a test example for the transport of a concentration in a deformed pipe subject to three-dimensional incompressible flow. The geometry of the pipe is illustrated in Figure 9 and a well developed velocity field is assumed to be given by solving the incompressible Navier-Stokes equations. Initially,

$$c(x, y, z, 0) = \begin{cases} 1, & \text{if} \quad r < R_0 \\ \\ 0, & \text{if} \quad r \geq R_0, \end{cases}$$

where $r = \sqrt{\left(\frac{x-2}{4}\right)^2 + y^2 + z^2}$ and $R_0 = 0.2$. In our computations, we set CFL $= 10$ and consider two unstructured meshes with tetrahedral finite elements as depicted in Figure 10. The corresponding

Table 3: Mesh statistics and CPU times (in seconds) for the problem of a passive transport in a deformed pipe using the P_1 elements, the P_2 elements and the slope limiters.

				CPU		
Mesh	# elements	# P_2 nodes	# P_1 nodes	P_1 elements	P_2 elements	Limiting
Mesh A	207729	304211	40591	3.314	12.541	13.453
Mesh B	472112	666689	85692	7.152	19.461	20.578

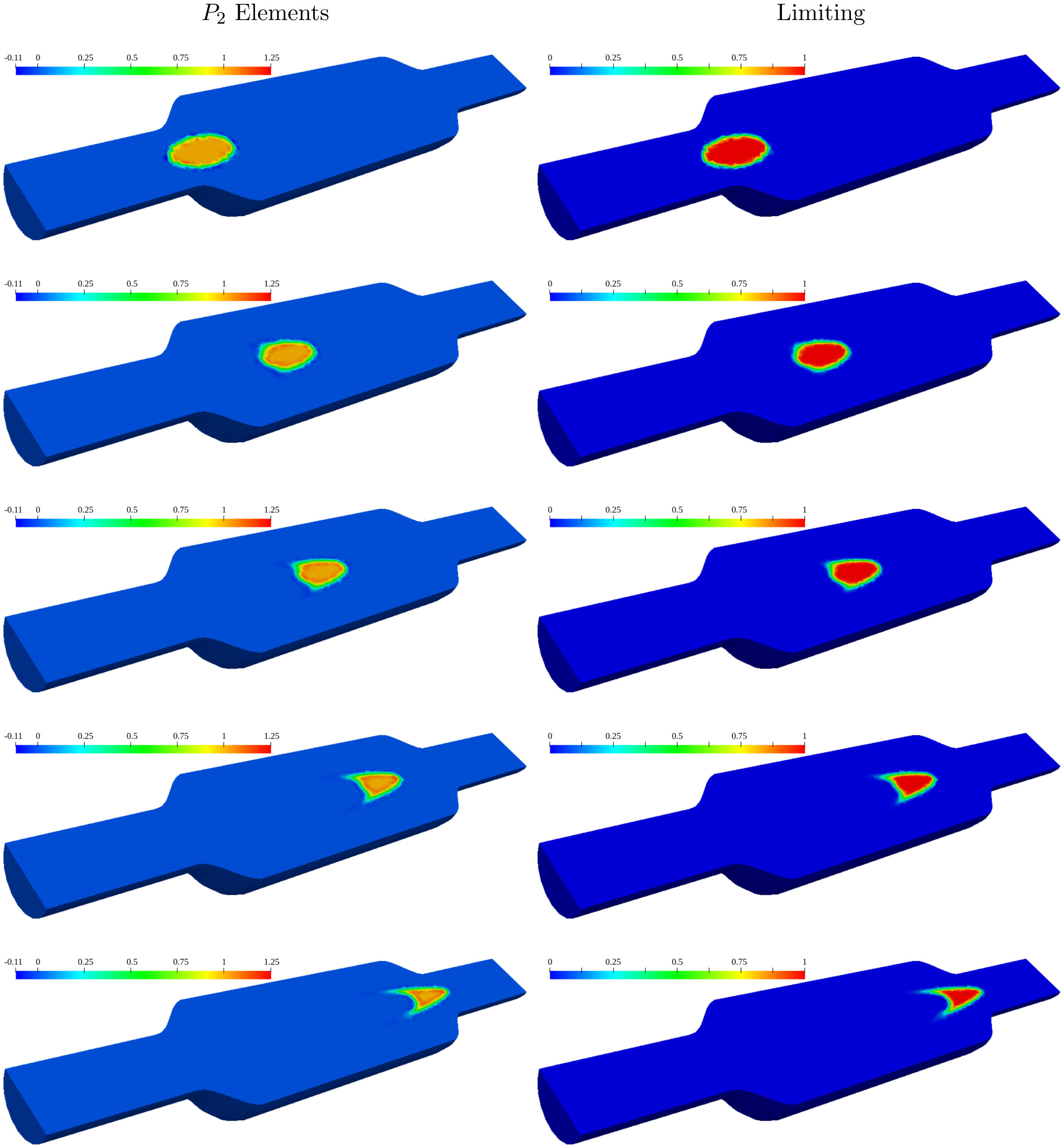

Figure 11: Numerical results obtained for passive transport in a deformed pipe using the P_2 elements (left column) and the slope limiters (right column) on Mesh A at five different instants. From top to bottom $t = 0.4\ s$, $1.5\ s$, $2\ s$, $3\ s$ and $4\ s$.

statistics of elements and nodes in P_1 and P_2 elements are listed in Table 3. Note that Mesh B is not included in Figure 10 because of its density which results in a heavily black plot.

Figure 11 illustrates the concentration patterns obtained at five different times, namely $t = 0.4\ s$, $1.5\ s$, $2\ s$, $3\ s$ and $4\ s$ using the P_2 elements and the proposed slope limiters. For better insight, only a lateral section of the pipe is used to display the results. For comparison purposes, Figure 12 depicts the one-dimensional cross-sections of the concentration at $y = z = 0$. It is easy to see from both figures,

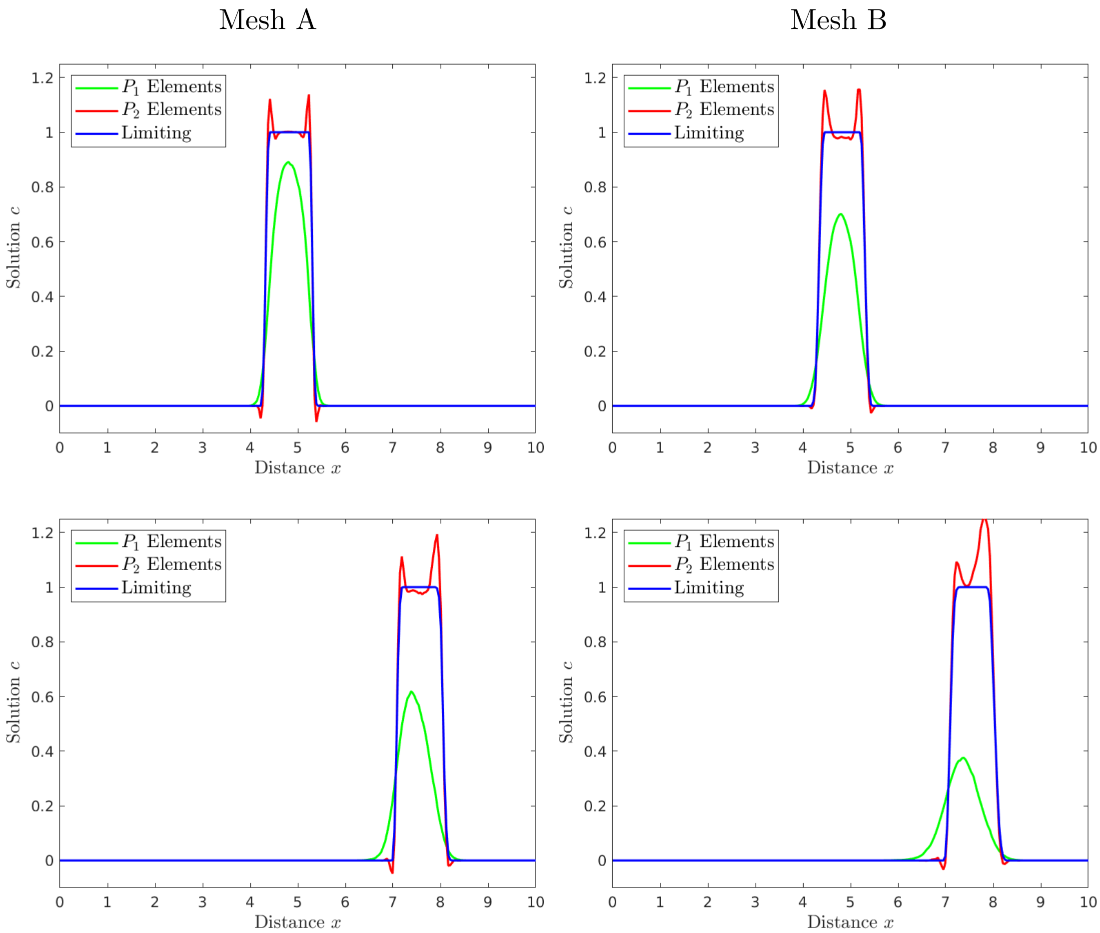

Figure 12: Cross-sections of the solution at $y = z = 0$ obtained for passive transport in a deformed pipe using the P_1 elements, the P_2 elements and the slope limiters on Mesh A (left column) and Mesh B (right column). Here, $t = 2\ s$ (first row) and $t = 4\ s$ (second row).

that solutions obtained using the Mesh B are more accurate than those obtained using the coarse Mesh A. The results obtained using the slope limiters exhibit a good shock resolution with a high accuracy in the smooth regions and without any non-physical oscillations near the shock areas. The comparison between the results obtained using P_2 and P_1 elements in Figure 12 illustrates large numerical dissipation in the results obtained using the P_1 elements and spurious oscillations in the results obtained using the P_2 elements. However, the results presented in the same figure for the slope limiters are free from non-physical oscillations and excessive numerical diffusion. From the results computed using the slope limiters we can observe that the complicated transport features in the deformed pipeline being well captured by the modified method of characteristics on unstructured finite elements. It is worth remarking that all these structures have been achieved using time steps larger than those required for Eulerian-based finite element methods solving convection-dominated problems. For the sake of completeness, we summarize in Table 3 the computational times in the considered methods. The clear indication from this table is that the CPU time employed by the P_2 elements and the slope limiters is approximately four times larger than in the P_1 elements for the same mesh. As can be observed, there is little differences between the CPU times in the P_2 elements and in the slope limiters.

4 Concluding remarks

A monotonicity-preserving modified method of characteristics on unstructured tetrahedral meshes is presented in this study for solving three-dimensional transport problems. This method exploits the interesting features offered by slope limiters to eliminate non-physical oscillations in the computed solutions near discontinuities and steep gradients. The proposed method combines the modified method of characteristics with a finite element discretization of the transport problems using unstructured grids. The main advantage of the proposed method is that, the advection terms which need special treatment in most Eulerian-based methods has been dealt with using the modified method of characteristics to interpret the transport nature of the equation under consideration. Slope limiters are accounted for in the method to reconstruct a monotone and essentially non-oscillatory solver for three-dimensional problems at minor additional cost. Here, a class of limiter functions is proposed based on linear and quadratic interpolation procedures using nodes of the finite element where departure points are localized. The favorable performance of the modified method of characteristics has been demonstrated using a series of numerical examples including a passive transport in three-dimensional pipeline flows. A comparison between the proposed method and the conventional modified method of characteristics using linear and quadratic finite elements were also performed in the current work. The obtained results using the proposed method show good solution resolution and less numerical dissipation compared to the results computed using the quadratic and linear elements, respectively. The computational results for transport in pipelines showed that it is possible to efficiently estimate the concentration transport with a computational cost significantly lower than solving the equations using the conventional finite element method. The proposed modified method of characteristics is promising and can be applied to different real world applications involving transport models where predicting the concentration can substantially benefit from the efficiency and accuracy of the proposed solver. Future work will concentrate on developing monotonicity-preserving modified method of characteristics for nonlinear convection-diffusion problems including the incompressible Navier-Stokes equations in three space dimensions.

References

[1] M. Abbas, Ahmad A. Majid, and J.Md Ali. Positivity-preserving rational bi-cubic spline interpolation for 3D positive data. *Applied Mathematics and Computation*, 234:460–476, 2014.

[2] R. Bermejo and J. Conde. A conservative quasi-monotone semi-Lagrangian scheme. *Monthly Weather Review*, 130(2):423–430, 2002.

[3] R. Bermejo and L. Saavedra. Modified Lagrange-Galerkin Methods to Integrate Time Dependent Incompressible Navier-Stokes Equations. *SIAM Journal on Scientific Computing*, 37(6):B779–B803, 2015.

[4] F. Bertrand, L. Demkowicz, J. Gopalakrishnan, and N. Heuer. Recent Advances in Least-Squares and Discontinuous Petrov-Galerkin Finite Element Methods. *Computational Methods in Applied Mathematics*, 19(3):395–397, 2019.

[5] Sh. Boroun and F. Larachi. Anomalous anisotropic transport of scalars in dilute ferrofluids under uniform rotating magnetic fields-mixing time measurements and ferrohydrodynamic simulations. *Chemical Engineering Journal*, 380:122504, 2020.

[6] A.N. Brooks and T.JR. Hughes. Streamline upwind/Petrov-Galerkin formulations for convection dominated flows with particular emphasis on the incompressible Navier-Stokes equations. *Computer methods in applied mechanics and engineering*, 32(1-3):199–259, 1982.

[7] A. Murrone C. Le Touze and H. Guillard. Multislope MUSCL method for general unstructured meshes. *Journal of Computational Physics*, 284:389–418, 2015.

[8] E.O.A. Carew, P. Townsend, and M.F. Webster. A Taylor-Petrov-Galerkin algorithm for viscoelastic flow. *Journal of non-newtonian fluid mechanics*, 50(2-3):253–287, 1993.

[9] Y. Chai, Z. Gong, W. Li, T. Li, Q. Zhang, Z. Zou, and Y. Sun. Application of smoothed finite element method to two-dimensional exterior problems of acoustic radiation. *International journal of computational methods*, 15(05):1850029, 2018.

[10] S.P. Cook, C.J. Budd, and T. Melvin. The moving mesh semi-Lagrangian MMSISL method. *Journal of Computational Physics*, 393:484–502, 2019.

[11] M.J. Crochet and V. Legat. The consistent streamline-upwind/Petrov-Galerkin method for viscoelastic flow revisited. *Journal of non-newtonian fluid mechanics*, 42(3):283–299, 1992.

[12] X.Y. Cui, S. Chang, and G.Y. Li. A two-step Taylor-Galerkin smoothed finite element method for lagrangian dynamic problem. *International Journal of Computational Methods*, 12(04):1540004, 2015.

[13] M. Dehghan. Numerical Solution of the Three-dimensional Advection-Diffusion Equation. *Applied Mathematics and Computation*, 150:5–19, 2004.

[14] J. Donea. A Taylor-Galerkin method for convective transport problems. *International Journal for Numerical Methods in Engineering*, 20(1):101–119, 1984.

[15] J. Douglas and T.F. Russell. Numerical methods for convection dominated diffusion problems based on combining the method of characteristics with finite elements or finite differences. *SIAM Journal on Numerical Analysis*, 19:871–885, 1982.

[16] M. El-Amrani and M. Seaid. Convergence and Stability of Finite Element Modified Method of Characteristics for the Incompressible Navier-Stokes equations. *Journal of Numerical Mathematics*, 15:101–135, 2007.

[17] M. El-Amrani and M. Seaid. Numerical simulation of natural and mixed convection flows by Galerkin-characteristics method. *International Journal for Numerical Methods in Fluids*, 53:1819–1845, 2007.

[18] M. El-Amrani and M. Seaid. A Finite Element Modified Method of Characteristics for Convective Heat Transport. *Numerical Methods for Partial Differential Equations*, 24:776–798, 2008.

[19] M. El-Amrani and M. Seaid. A Galerkin-characteristics method for large-eddy simulation of turbulent flow and heat transfer. *SIAM Journal on Scientific Computing*, 30:2734–2754, 2008.

[20] M. El-Amrani and M. Seaid. An essentially non-oscillatory semi-Lagrangian method for tidal flow simulations. *International Journal for Numerical Methods in Engineering*, 81(7):805–834, 2010.

[21] M.J. Peng H. Cheng and Y.M. Cheng. A hybrid improved complex variable element-free Galerkin method for three-dimensional advection-diffusion problems. *Engineering Analysis with Boundary Elements*, 97:39–54, 2018.

[22] M. Hedayati-Dezfooli and W.H. Leong. An experimental study of coupled heat and moisture transfer in soils at high temperature conditions for a medium coarse soil. *International Journal of Heat and Mass Transfer*, 137:372–389, 2019.

[23] T. JR. Hughes, L. P. Franca, and G. M. Hulbert. A new finite element formulation for computational fluid dynamics: Viii. The Galerkin/least-squares method for advective-diffusive equations. *Computer methods in applied mechanics and engineering*, 73(2):173–189, 1989.

[24] J. Isenberg and Ch. Gutfinger. Heat transfer to a draining film. *International Journal of Heat and Mass Transfer*, 16(2):505–512, 1973.

[25] M.R. Kaazempur-Mofrad and C.R. Ethier. An efficient characteristic Galerkin scheme for the advection equation in 3-D. *Computer methods in applied mechanics and engineering*, 191(46):5345–5363, 2002.

[26] L. Ali Khan and P.L.F. Liu. An operator splitting algorithm for the three-dimensional advection-diffusion equation. *International Journal for Numerical Methods in Fluids*, 28:461–476, 1998.

[27] D. Kuzmin, M. Möller, and S. Turek. Multidimensional FEM-FCT schemes for arbitrary time stepping. *International journal for numerical methods in fluids*, 42(3):265–295, 2003.

[28] T. Ma and Y. Ge. A blended compact difference (BCD) method for solving 3D convection-diffusion problems with variable coefficients. *International Journal of Computational Methods*, 17(06):1950022, 2020.

[29] N.S. Park and J. A. Liggett. Application of Taylor-least squares finite element to three-dimensional advection-diffusion equation. *International Journal for Numerical Methods in Fluids*, 13:759–773, 1991.

[30] O. Pironneau. On the transport-diffusion algorithm and its applications to the Navier-Stokes equations. *Numerische Mathematik*, 38:309–332, 1982.

[31] H. Rui and M. Tabata. A Mass-Conservative Characteristic Finite Element Scheme for Convection-Diffusion Problems. *Journal of Scientific Computing*, 43:416–432, 2010.

[32] T. Sato, Ch. Batty, T. Igarashi, and R. Ando. Spatially adaptive long-term semi-Lagrangian method for accurate velocity advection. *Computational Visual Media*, 4(3):223–230, 2018.

[33] M. Seaid. On the quasi-monotone modified method of characteristics for transport-diffusion problems with reactive sources. *Computational Methods in Applied Mathematics Comput. Methods Appl. Math.*, 2(2):186–210, 2001.

[34] M. Seaid. Semi-Lagrangian integration schemes for viscous incompressible flows. *Computational Methods in Applied Mathematics Comput. Methods Appl. Math.*, 2(4):392–409, 2002.

[35] R. Strehl, A. Sokolov, D. Kuzmin, D. Horstmann, and S. Turek. A positivity-preserving finite element method for chemotaxis problems in 3D. *Journal of Computational and Applied Mathematics*, 239:290–303, 2013.

[36] L. L. Takacs. A two-step scheme for the advection equation with minimized dissipation and dispersion errors. *Monthly Weather Review*, 113(6):1050–1065, 1985.

[37] C. Temperton and A. Staniforth. An efficient two-time-level Galerkin-characteristics semi-implicit integration scheme. *Quarterly Journal of the Royal Meteorological Society*, 113:1025–1039, 1987.

[38] D. Xiu and G.E. Karniadakis. A Galerkin-characteristics high-order method for Navier-Stokes equations. *Journal of Computational Physics*, 172:658–684, 2001.

[39] Y. Xu. Similarity Solution and Heat Transfer Characteristics for a Class of Nonlinear Convection-Diffusion Equation with Initial Value Conditions. *Mathematical Problems in Engineering*, 2019, 2019.

[40] S.T. Zalesak. Fully multidimensional flux-corrected transport algorithms for fluids. *Journal of computational physics*, 31(3):335–362, 1979.

[41] Y. Zhai, X. Feng, and D. Lu. A novel method to deduce high-order compact difference scheme for the three dimensional semilinear convection-diffusion equation with variable coefficients. *Numerical Heat Transfer*, B 63 (5):425–455, 2013.

[42] Z.L. Zhang, T. Ma, M.B. Liu, and D. Feng. Numerical study on high velocity impact welding using a modified SPH method. *International Journal of Computational Methods*, 16(02):1846001, 2019.